

# Water vapor retrievals using Moderate Resolution Imaging Spectroradiometer (MODIS) near-infrared channels

Bo-Cai Gao

Remote Sensing Division, Naval Research Laboratory, Washington, D. C., USA

Yoram J. Kaufman

Climate and Radiation Branch, NASA Goddard Space Flight Center, Greenbelt, Maryland, USA

Received 8 October 2002; revised 7 February 2003; accepted 24 March 2003; published 10 July 2003.

[1] At present, two Moderate Resolution Imaging Spectroradiometer (MODIS) instruments on board the NASA Terra and Aqua Spacecraft platforms are operational for global remote sensing of the land, ocean, and atmosphere. In this paper, we describe an algorithm for water vapor derivations using several MODIS near-IR channels. The derivations are made over areas that have reflective surfaces in the near-IR, such as clear land areas, clouds, and oceanic areas with Sun glint. The algorithm relies on observations of water vapor attenuation of near-IR solar radiation reflected by surfaces and clouds. Techniques employing ratios of water vapor absorbing channels centered near 0.905, 0.936, and 0.940  $\mu\text{m}$  with atmospheric window channels at 0.865 and 1.24  $\mu\text{m}$  are used. The ratios partially remove the effects of variation of surface reflectance with wavelengths and result in the atmospheric water vapor transmittances. The column water vapor amounts are derived from the transmittances based on theoretical calculations and using lookup table procedures. Typical errors in the derived water vapor values are in the range between 5% and 10%. The daily “pixel-based” near-IR water vapor product, which is a standard MODIS level 2 data product, at the 1-km spatial resolution of the MODIS instrument, and the daily, 8-day, and monthly near-IR water vapor products, which are standard MODIS level 3 products, at a  $1^\circ$  by  $1^\circ$  latitude-longitude grid globally are now routinely produced at a NASA computing facility. We present samples of water vapor images and comparisons to ground-based measurements by microwave radiometers. **INDEX TERMS:** 0315 Atmospheric Composition and Structure: Biosphere/atmosphere interactions; 0325 Atmospheric Composition and Structure: Evolution of the atmosphere; 1640 Global Change: Remote sensing; **KEYWORDS:** water vapor, remote sensing, MODIS, terrestrial atmosphere

**Citation:** Gao, B.-C., and Y. J. Kaufman, Water vapor retrievals using Moderate Resolution Imaging Spectroradiometer (MODIS) near-infrared channels, *J. Geophys. Res.*, 108(D13), 4389, doi:10.1029/2002JD003023, 2003.

## 1. Introduction

[2] Historically, remote sensing of water vapor profiles from space was made using IR emission channels. The results depended in part on the initial guess for the temperature and moisture profiles used in the inversion [Susskind *et al.*, 1984]. Column water vapor amounts over the ocean were retrieved from IR emission channels in the 11–13  $\mu\text{m}$  spectral region using “split window” techniques [Chesters *et al.*, 1983] and from microwave emission measurements [Prabhakara *et al.*, 1982; Ferraro *et al.*, 1996]. The “split window” techniques also work well over land areas covered by green vegetation. When the apparent surface temperature, which is a function of surface emissivity and skin temperature, is about equal to the average temperature of the boundary layer, where most of the water vapor usually

resides, infrared and microwave remote sensing will not be sensitive to the boundary layer water vapor. In recent years, a number of papers have reported water vapor retrieval algorithms, which use backscattered solar radiation near 1  $\mu\text{m}$  measured with aircraft and satellite instruments [e.g., Conel *et al.*, 1988; Gao and Goetz, 1990; Frouin *et al.*, 1990; Kaufman and Gao, 1992; Borel *et al.*, 1996; Bouffies *et al.*, 1997; Thai and Schonermark, 1998; Vesperini *et al.*, 1999].

[3] The MODIS instruments currently onboard the NASA Earth Observing System (EOS) Terra and Aqua Spacecrafts are NASA facility instruments [Salomonson *et al.*, 1989; King *et al.*, 1992; Asrar and Greenstone, 1995] designed for global monitoring of the land, ocean, and atmosphere. Three near-IR channels located within the 0.94- $\mu\text{m}$  water vapor band absorption region were implemented on MODIS for water vapor remote sensing. The implementation of the two water vapor channels centered at 0.905 and 0.94  $\mu\text{m}$  was largely based on the work of Gao and Goetz [1990] and Kaufman and Gao [1992] with water

**Table 1.** Positions and Widths of Five MODIS Near-IR Channels Used in Water Vapor Retrievals

MODIS Channel	Position, $\mu\text{m}$	Width, $\mu\text{m}$
2	0.865	0.040
5	1.240	0.020
17	0.905	0.030
18	0.936	0.010
19	0.940	0.050

vapor retrievals from high spatial resolution hyperspectral imaging data collected by the Airborne Visible Infrared Imaging Spectrometer (AVIRIS) [Vane *et al.*, 1993; Green *et al.*, 1998] from a NASA ER-2 aircraft at an altitude of 20 km. In this paper, we describe the algorithm for deriving column water vapor amounts from measurements of near-IR solar radiation reflected by Earth's surfaces or clouds with the MODIS instruments.

## 2. Instrument Characteristics

[4] The MODIS instrument has 36 channels covering the spectral region between 0.4 and 15  $\mu\text{m}$ . Five near-IR channels in the 0.8–1.3  $\mu\text{m}$  spectral region are useful for remote sensing of water vapor. The positions and widths of these channels from the original MODIS design specifications are given in Table 1 and illustrated in Figure 1. Two atmospheric water vapor transmittance spectra for the tropical and subarctic winter models [Kneizys *et al.*, 1988] with a solar zenith angle of 45 degrees and a nadir-looking geometry are also shown in Figure 1. The channels at 0.865 and 1.24  $\mu\text{m}$  positioned to avoid atmospheric gaseous absorption are for remote sensing of vegetation and clouds. The channels at 0.936, 0.940, and 0.905  $\mu\text{m}$  are water vapor absorption channels with decreasing absorption coefficients. The strong absorption channel at 0.936  $\mu\text{m}$  is most useful for dry conditions, while the weak absorption channel at 0.905  $\mu\text{m}$  is most useful for very humid conditions, or low solar elevation.

## 3. Algorithm Descriptions

[5] In this section we describe an algorithm for deriving column water vapor amounts from MODIS near-IR data from both the theoretical and practical points of view.

### 3.1. Theoretical Description

[6] The remote sensing method is based on detecting the absorption by water vapor of the reflected solar radiation after it has been transmitted down to the surface, reflected at the surface, and transmitted up through the atmosphere to the sensor. The equivalent total vertical amount of water vapor can be derived from a comparison between the reflected solar radiation in the absorption channel, and the reflected solar radiation in nearby nonabsorption channels. Descriptions of techniques for water vapor remote sensing using near-IR channels were previously reported [e.g., Gao and Goetz, 1990; Frouin *et al.*, 1990; Kaufman and Gao, 1992; Gao *et al.*, 1992; Borel *et al.*, 1996; Thai and Schonermark, 1998; Vesperiini *et al.*, 1999]. Below we describe the retrieving techniques relevant to the MODIS implementation.

[7] The solar radiation between 0.86 and 1.24  $\mu\text{m}$  on the Sun-surface-sensor path is subjected to atmospheric water vapor absorption, aerosol scattering, and surface reflection. In order to derive column water vapor from measurements of solar radiation reflected by the surface, the absorption and scattering properties of the atmosphere and the surface near 1  $\mu\text{m}$  must be taken into consideration.

#### 3.1.1. Atmospheric Absorption and Scattering in the 0.86–1.24 $\mu\text{m}$ Range

[8] The radiance at a downward looking satellite sensor can be approximated [Hansen and Travis, 1974; Fraser and Kaufman, 1985] as

$$L_{\text{Sensor}}(\lambda) = L_{\text{Path}}(\lambda) + [\mu_0 E_0(\lambda)/\pi] T(\lambda) \rho(\lambda) \quad (1)$$

where  $\lambda$  is wavelength,  $L_{\text{Sensor}}(\lambda)$  the radiance at the sensor,  $L_{\text{Path}}(\lambda)$  the path scattered radiance,  $\mu_0$  the cosine of solar zenith angle,  $E_0(\lambda)$  the extra-terrestrial solar flux,  $T(\lambda)$  the total atmospheric transmittance, which is equal to the product of the atmospheric transmittance from the Sun to the Earth's surface and that from the surface to the satellite sensor, and  $\rho(\lambda)$  the surface bi-directional reflectance. Equation (1) is simplified in a sense that photons that are reflected from the surface more than once are being ignored. This feedback mechanism involves back scattering to the surface by the atmosphere. Because aerosol optical thicknesses are typically small in the near-IR region, the feedback effect is usually small. The second term on the right hand side of equation (1) is the directly reflected solar radiation.  $L_{\text{Direct}}$  is used to represent this component. The term  $\pi L_{\text{Sensor}}(\lambda)/[\mu_0 E_0(\lambda)]$  is defined as the apparent reflectance  $\rho^*(\lambda)$  in this paper.

[9] The term  $T(\lambda)$  contains information about the total amount of water vapor in the combined Sun-surface-sensor path.  $E_0(\lambda)$  is a known quantity. Near 1  $\mu\text{m}$ , Rayleigh scattering is negligible and the main contribution to  $L_{\text{Path}}(\lambda)$  is scattering by aerosols.  $L_{\text{Path}}(\lambda)$  in the 1  $\mu\text{m}$  region is usually a few percent of the direct reflected solar radiation. Because most aerosols are located in the lower 2 km of the atmosphere and the same is true for atmospheric water vapor, the single and multiple scattered radiation by aero-

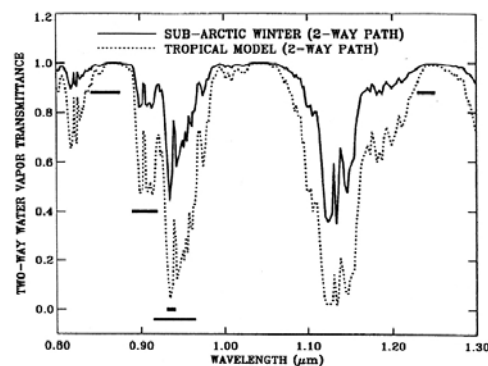


**Figure 1.** Positions and widths of five MODIS near-IR channels marked in thick horizontal bars, and two-way atmospheric water vapor transmittance spectra for the tropical and subarctic winter models in LOWTRAN-7 [Kneizys *et al.*, 1988] with a solar zenith angle of 45 degrees and a nadir-looking geometry.

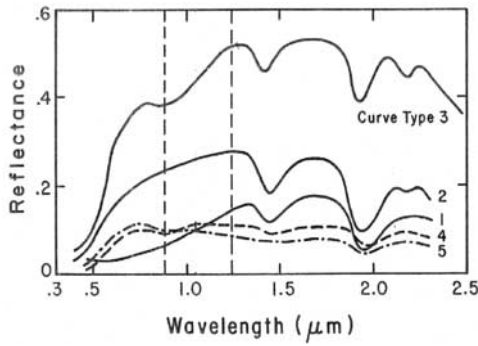


**Figure 2.** Typical soil reflectance curves for five major soil types [Condit, 1970; Stoner and Baumgartner, 1980]: (1) organic-dominated, moderately fine texture; (2) organic-affected, moderately coarse texture; (3) iron-dominated laterite-type soil; (4, 5) iron- and organic-rich soil, respectively.

soils is also subjected to water vapor absorption. As a result,  $L_{Path}(\lambda)$  contains water vapor absorption features [Gao and Goetz, 1990]. We assume that  $L_{Path}(\lambda)$  can be treated approximately as an unspecified fraction of direct reflected solar radiation when the aerosol concentrations are low. With this assumption we can derive column water vapor amounts from satellite data without the need for modeling the single and multiple scattering effects.

### 3.1.2. Surface Reflectances Near 1 $\mu\text{m}$

[10] MODIS images the land, ocean and clouds. Most land is either covered by soils, rocks, vegetation, snow, or ice. If the surface reflectance is either constant or varies in a linear fashion with wavelength, we can use a two- or three-channel ratio algorithm for water vapor retrievals. Figure 2 shows reflectance curves of five major types of soil [Condit, 1970; Stoner and Baumgardner, 1980]. The reflectances between 0.85 and 1.25  $\mu\text{m}$  change approximately linearly with wavelength. Similar linearity is observed in reflectance spectra of common rocks and minerals. The largest deviation from linearity is observed in reflectance spectra of iron-rich soils and minerals. These materials have broad electronic bands, which are related to the  $\text{Fe}^{3+}$  transition and are centered near 0.86  $\mu\text{m}$ . Curve 3 in Figure 2 shows such a broad band feature in the spectral region between approximately 0.8 and 1.25  $\mu\text{m}$ . Figure 3 shows vegetation and snow reflectance spectra [Bowker et al., 1985] normalized near 0.86  $\mu\text{m}$ . The vegetation spectrum has liquid water bands centered at approximately 0.98 and 1.20  $\mu\text{m}$ . The snow spectrum has ice absorption bands centered approximately at 1.04 and 1.24  $\mu\text{m}$ . For comparison, Figure 3 also shows a calculated water vapor transmittance spectrum. The positions of water vapor, liquid water and ice absorption bands are shifted relative to each other. The shifting of the vibrational bands is due to increases in intermolecular forces as the water molecules become more organized in the liquid and solid states.

[11] The ocean is highly absorbing at wavelengths longer than 0.8  $\mu\text{m}$ . The MODIS near-IR channels receive very little radiances over the dark ocean surfaces. Reliable water vapor retrievals over the dark ocean surfaces from the near-IR channel measurements cannot be made because of poor signal-to-noise ratios. However, fog, stratus clouds, or Sun

glint regions are very bright and spectrally flat over the 0.85–1.25  $\mu\text{m}$  spectral region.

### 3.1.3. Transmittance Derivation Using Channel Ratio Techniques

[12] The reflectance values at a given wavelength are quite different for different types of surfaces, as seen from Figures 2 and 3. Therefore it is not possible to get the water vapor transmittances (see equation (1)) from radiances of individual absorption channels. However, if the surface reflectances are constant with wavelength, a two-channel ratio of an absorption channel with a window channel gives the water vapor transmittance of the absorption channel. For example, the transmittance of the channel at 0.94  $\mu\text{m}$  can be expressed as

$$T_{\text{obs}}(0.94 \mu\text{m}) = \rho^*(0.94 \mu\text{m}) / \rho^*(0.865 \mu\text{m}), \quad (2)$$

if the surface reflectances are constant with wavelength and if the path radiances can be treated as small fractions of directly reflected solar radiances.

[13] If surface reflectances vary linearly with wavelength, a three-channel ratio of an absorption channel with a combination of two window channels gives the water vapor transmittance of the absorption channel. For example, the transmittance of the channel at 0.94  $\mu\text{m}$  can be written as

$$T_{\text{obs}}(0.94 \mu\text{m}) = \rho^*(0.94 \mu\text{m}) / [C_1 * \rho^*(0.865 \mu\text{m}) + C_2 * \rho^*(1.24 \mu\text{m})], \quad (3)$$

where  $C_1$  is equal to 0.8, and  $C_2$  0.2. The denominator in equation (3) is, in fact, the estimated 0.94- $\mu\text{m}$  reflectance in the absence of water vapor absorption based on the two atmospheric window channels centered at 0.865 and 1.24  $\mu\text{m}$  through linear interpolation.

[14] For most of the soil spectra in Figure 2 (except the iron-rich soil spectrum) with quite linear spectral dependence in the 0.8–1.3  $\mu\text{m}$  wavelength region, the denominator in equation (3) would properly predict the surface reflectances at 0.94  $\mu\text{m}$ , and equation (3) would give excellent estimates of water vapor transmittance for the 0.94- $\mu\text{m}$  channel from MODIS data acquired over these types of soils. For the iron-rich soil spectrum in Figure 2

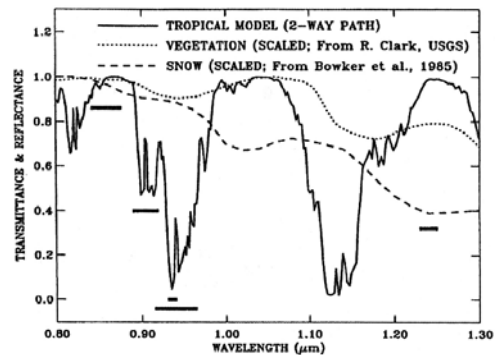


**Figure 3.** A two-way transmittance spectrum of atmospheric water vapor and reflectance spectra (scaled) of green vegetation and snow. The band centers of water vapor, liquid water, and ice are relatively shifted by approximately 50 nm.

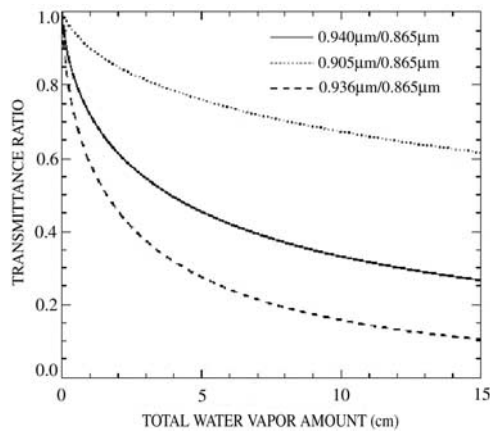


**Figure 4.** Examples of simulated transmittance ratios of two channels (absorption channel/window channel) as a function of total water vapor amount in the Sun-surface-sensor path.

and the vegetation and snow reflectance spectra (scaled) in Figure 3, although they do not vary linearly with wavelength in the 0.8–1.3  $\mu\text{m}$  wavelength region, the denominator in equation (3) would also allow reasonable estimates of surface reflectances at 0.94  $\mu\text{m}$  with errors typically less than about 4%, and equation (3) would still give reasonable estimates of water vapor transmittances for the 0.94- $\mu\text{m}$  channel from MODIS data acquired over iron-rich soils, green vegetation, and snow. Further discussion of the errors associated with the assumption of linearity of surface reflectances in the 0.8–1.3  $\mu\text{m}$  is included in section 5.

### 3.1.4. Water Vapor Retrievals Over Land and Oceanic Areas With Sun Glint

[15] Both the two-channel and three-channel ratio techniques are used to derive atmospheric transmittances of the absorption channels, and subsequently the column water vapor amounts over clear land areas and extended oceanic areas with sun glint. The three-channel ratio technique is used for water vapor derivations over clear land pixels, while the two-channel ratio technique is used over oceanic areas with sun glint. The two-channel and three-channel ratios are calculated from radiances of the five MODIS channels centered at 0.865, 0.905, 0.936, 0.94, and 1.24  $\mu\text{m}$ . Lookup tables containing values of two-channel and three-channel ratios and total amounts of water vapor were precomputed using a line-by-line atmospheric transmittance code (W. Ridgway, personal communications 2001), the HITRAN2000 spectroscopic database [Rothman *et al.*, 1998], and the actual filter transmission functions of the five MODIS channels. Figure 4 shows examples of the simulated two-channel ratios (absorption channel/window channel) as a function of total water vapor amount in the Sun-surface-sensor path. The combined two-way water vapor amount is derived from values of two-channel and three-channel ratios calculated from the MODIS data using a table-searching procedure. The derived total water vapor amount,  $W^*$ , is then converted to the vertical column water vapor amount,  $W$ , based on the solar and the observational geometries using the equation

$$W = W^* / [1 / \cos(\theta_s) + 1 / \cos(\theta_v)], \quad (4a)$$

where  $\theta_s$  is the solar zenith angle, and  $\theta_v$  the view zenith angle.

### 3.1.5. Water Vapor Retrievals Over Clouds

[16] When clouds are present, the MODIS channels in the 0.8–2.5  $\mu\text{m}$  region contain information about absorptions due to water vapor above and within clouds. This is illustrated in Figure 5, in which sample cumulus and cirrus cloud spectra over water surfaces measured with the AVIRIS instrument [Vane *et al.*, 1993] from an ER-2 aircraft at an altitude of 20 km. The band passes of a few MODIS channels are marked in thick horizontal bars. Because cirrus clouds are much higher than cumulus clouds, the depth of the absorption feature of the 0.94- $\mu\text{m}$  water vapor band for the cirrus spectrum is much smaller than that for the cumulus spectrum.

[17] In the presence of optically thick clouds, the two-channel ratios (see equation (2)) provide information about absorptions due to water vapor molecules on the Sun-cloud-sensor path. The absorption effect is enhanced slightly due to multiple scattering of solar radiation within clouds. In order to infer the actual number of water vapor molecules that interacted with solar radiation, the cloud top height must be known, because molecular absorption depends on atmospheric pressures. The cloud top heights for low level water clouds are difficult to determine accurately from passive remote sensing data. Therefore we retrieve “effective” column water vapor amounts from the two-channel ratio values for pixels with thick water clouds by assuming that the cloud top heights are at the sea level. These effective water vapor amounts can, in principle, be used to estimate the water vapor absorption effects in MODIS channels shorter than about 4  $\mu\text{m}$ , provided that water vapor transmittances for different MODIS channels are calculated with the same assumption of cloud top heights being at the sea level. The cloud top heights for upper level thick cirrus clouds can be retrieved from MODIS IR emission channels [Menzel *et al.*, 1992; King *et al.*, 1992]. From the two-channel ratio values plus the estimated IR cloud heights, the column water vapor amount over thick cirrus pixels can be retrieved.

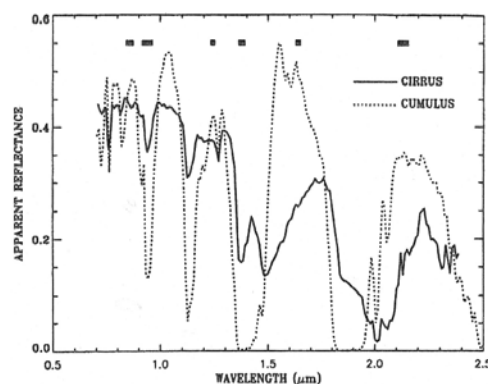


**Figure 5.** Sample cumulus and cirrus cloud spectra over water surfaces measured with the NASA/JPL Airborne Visible Infrared Imaging Spectrometer from an ER-2 aircraft at 20 km. Because cirrus clouds are much higher than cumulus clouds, the peak absorption feature of the 0.94- $\mu\text{m}$  water vapor band for the cirrus spectrum is much smaller than that for the cumulus spectrum.

[18] In the presence of optically thin clouds (usually ice clouds), an index of column water vapor amount above and within cirrus clouds can be established. Our recent analysis of AVIRIS data acquired over water surfaces indicates that the ratio of the radiance from the 0.94- $\mu\text{m}$  channel against the radiance from the 0.865- $\mu\text{m}$  channel provides information about water vapor above and within cirrus clouds. Because the water surface away from sun glint regions is black above 0.8  $\mu\text{m}$ , it has no contribution to the two-channel ratio. The sensitivities of MODIS IR channels near 14  $\mu\text{m}$  are not sufficiently high for reliable detection of thin cirrus clouds with effective IR emissivities less than about 0.04. The estimation of the heights of such thin cirrus clouds using CO<sub>2</sub> slicing techniques [Zhang and Menzel, 2002] is not possible. For slightly thicker cirrus clouds, the CO<sub>2</sub> slicing technique can sometimes successively estimate the heights of such clouds, but often has a tendency to underestimate the height of such clouds due to intrinsic absorption, emission, and partial transparent nature of cirrus clouds. On the basis of these considerations, we have concluded that thin cirrus cloud heights will have to be assumed at a few discrete height levels based on climatology. From the two-channel ratios and the assumed cirrus heights, the upper level water vapor index can, in principle, be established.

### 3.2. Practical Implementation

[19] Our level 2 near-IR water vapor algorithm requires input data sets from standard MODIS data cubes and associated ancillary data. The inputs from MODIS data cubes are radiances of five MODIS channels centered at 0.865, 0.905, 0.936, 0.94, and 1.24  $\mu\text{m}$ . The inputs from ancillary data are solar zenith angle, view zenith angle, relative azimuth angle between the solar and viewing directions, cloud mask, land-water flag, surface elevation, and surface temperature. The required angular information is for converting the total two-way path water vapor amount to the vertical column amount. The cloud mask is used to indicate whether a pixel is clear or cloudy. The land-water flag is used to show if the pixel is over land or water. Both the cloud mask and land-water flag are used in our selection of either the two-channel or the three-channel ratio method in the retrievals. Because molecular absorption depends on pressure, surface elevations in digital form are used in our algorithm for pressure scaling of water vapor amounts (the same scheme as that used in LOWTRAN7 [Kneizys *et al.*, 1988] and MODTRAN [Berk *et al.*, 1989; Anderson *et al.*, 2000]). Surface temperature is used in the selection of an appropriate model atmosphere for the retrieval.

[20] Atmospheric water vapor has very different absorption coefficients over the band passes of MODIS channels centered near 0.936, 0.940, and 0.905  $\mu\text{m}$ . As a result, the three channels have different water vapor sensitivities under the same atmospheric condition. The strong absorption channel at 0.936  $\mu\text{m}$  is most sensitive under dry conditions, while the weak absorption channel at 0.905  $\mu\text{m}$  is most sensitive under humid conditions. Under a given atmospheric condition, the derived water vapor values from the three channels can be different. A mean water vapor value ( $W$ ) is obtained according to the equation:

$$W = f_1 W_1 + f_2 W_2 + f_3 W_3, \quad (4b)$$

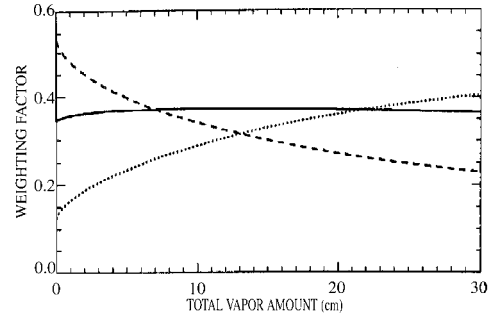


**Figure 6.** The normalized weighting factors as a function of total precipitable water vapor. Solid line is for the wide 0.94- $\mu\text{m}$  channel, dashed line is for the narrow 0.936- $\mu\text{m}$  channel, and the dotted line is for the 0.905- $\mu\text{m}$  channel.

where  $W_1$ ,  $W_2$ , and  $W_3$  are water vapor values derived from the 0.936, 0.940, and 0.915  $\mu\text{m}$  channels, respectively, and  $f_1$ ,  $f_2$ , and  $f_3$  are the corresponding weighting functions. Our currently adopted weighting functions are based on the sensitivity of the transmission ( $T_i$ ) in each of the channels ( $i$ ) to the total precipitable water vapor ( $W$ ):  $\eta_i = |\Delta T_i / \Delta W|$ . The weighting functions,  $f_i$ , are defined as the normalized values of  $\eta_i$ :

$$f_i = \eta_i / (\eta_1 + \eta_2 + \eta_3); \quad \eta_i = |\Delta T_i / \Delta W| \quad (5)$$

These weighting functions are computed numerically from simulated curves of transmittances versus precipitable water. Figure 6 shows the dependence of  $f_i$  on the total precipitable water vapor for the three filters.

[21] The output from our level 2 near-IR water vapor algorithm includes the column water vapor amount on a pixel-by-pixel basis and an associated quality assurance parameter that indicates whether a pixel is clear or cloudy. The column water vapor amounts are derived over clear land areas of the globe, and above clouds over both land and ocean. Water vapor estimates are also made over extended glint oceanic areas. In addition to the level 2 near-IR water vapor product, the level 3 near-IR water vapor products for clear areas and cloudy areas are produced on the daily, 8-day, and monthly mean basis at a  $1^\circ \times 1^\circ$  latitude-longitude equal angle grid globally.

## 4. Results

[22] The algorithm has been used for operational retrievals of column water vapor amounts from MODIS data. The level 2 and level 3 data products have been stored at the Goddard Distributed Archive Center in Greenbelt, Maryland. Researchers interested in the products can obtain them from this data center. Below we show a few examples of the level 2 “pixel-based” water vapor images and the level-3 “monthly mean” water vapor images.

### 4.1. A Sample Level 2 Water Vapor Image From Terra MODIS

[23] The Terra MODIS instrument was launched into orbit on 18 December 1999. It started to collect scientific data in late February of 2000. Figure 7 shows an example of water vapor retrievals from the Terra MODIS near-IR

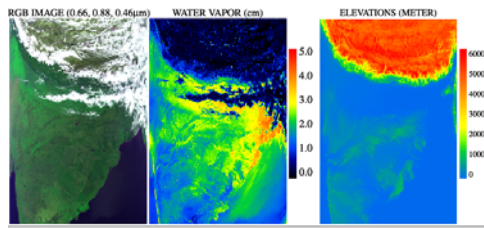


**Figure 7.** An example of water vapor retrievals from the Terra MODIS near-IR channels. The left panel shows a false color image of a MODIS scene covering the Indian continent and Himalayas mountains. The middle panel shows the water vapor image derived from MODIS near-IR channels. The right panel shows the surface elevation image for the scene. The MODIS data were acquired on 2 March 2000.

channels located within and around the 0.94- $\mu\text{m}$  water vapor band. The left panel shows a false color image processed from the MODIS channels centered at 0.645  $\mu\text{m}$  (red), 0.86  $\mu\text{m}$  (false green), and 0.47  $\mu\text{m}$  (blue). The lower left part of the scene covers a major portion of the Indian Continent. The lower right part covers a portion of the Bay of Bengal. The upper part of the scene covers Nepal. The MODIS data were measured on 2 March 2000 at UTC 0525. The middle panel shows the column water vapor image derived from the MODIS data. The right panel shows an image of surface elevations for the scene. By comparing the middle panel image with the right panel image, it is seen that over the high elevation Himalayas mountain regions, the water vapor amounts are quite small (<1 cm). Over the low elevation Indian Continent, the water vapor amounts are significantly larger. The high elevation Himalayas mountains block the northward movement of water vapor originated from the Bay of Bengal, and force the water vapor to remain in the Indian Continent.

#### 4.2. A Sample Level 2 Water Vapor Image From Aqua MODIS

[24] The MODIS instrument onboard the Aqua spacecraft was launched into orbit on May 4, 2002. The Aqua MODIS started to collect scientific data in late June of 2002. Figure 8 shows a sample of water vapor derivations from the Aqua MODIS data. In Figure 8a we show a color image processed from the MODIS channels centered at 0.645  $\mu\text{m}$  (red), 0.55  $\mu\text{m}$  (green), and 0.47  $\mu\text{m}$  (blue). The top part of the scene covers major portions of Spain and Portugal. The bottom part covers parts of Morocco and Algeria. Atlantic Ocean is seen in the left part of the image. The Mediterranean Sea is seen in the right part of the image. The Aqua MODIS data were acquired on 17 July 2002 at UTC 1350. In Figure 8b we show the column water vapor image derived from the Aqua MODIS data set. The areas over land and close to the land-water boundaries have higher concentrations of water vapor. The desert areas in the bottom right portions of the scene have far less water vapor than the coastal areas. It is quite easy to see spatial variations of water vapor from this image.

#### 4.3. Sample Level 3 Water Vapor Images Over the United States From Terra MODIS

[25] Through analysis of our level 3 daily, 8-day, and monthly mean water vapor images at a  $1^\circ \times 1^\circ$  latitude-

longitude equal angle grid, we have found that the monthly mean level 3 images allow easy observations of seasonal variations of water vapor distributions. Figure 9a shows a level 3 water vapor image over the continental United States, portions of Mexico and Canada for January of 2001. In this winter month, most parts of the United States have column water vapor amounts less than 1.5 cm. The State of Florida and the southern part of Texas have column water vapor amounts between approximately 2 and 3 cm. Figure 9b is a level 3 water vapor image over the same area but for July of 2001. The Rocky Mountain areas have column water vapor values less than about 2 cm in the summer month. Many states in central United States have high concentrations of water vapor originating from the Gulf of Mexico. The moisture even reaches Canada through North Dakota and Minnesota. The high concentrations of moisture over the western part of Mexico are due to water vapor originated from the Pacific Ocean. The patterns of water vapor distributions for the summer month are drastically different from those for the winter month.

#### 4.4. Sample Level 3 Water Vapor Images Over Australia From Terra MODIS

[26] The level 3 monthly mean near-IR water vapor images can also be used to study annual variations of water vapor distributions. Figure 10 shows an example of such studies. In Figure 10a we show the level 3 water vapor image over Australia for January 2001. January is a summer month in the Southern Hemisphere. The northern part of Australia is in the tropical region. Column water vapor amounts over this region are typically in the 4–6 cm range. The southeastern parts of Australia typically have column water vapor amounts between 2 and 3 cm. Figure 10b shows the water vapor image over Australia for the same month but for the year of 2002, an El Nino year. By comparing Figure 10b with Figure 10a, it is seen that column water vapor amounts in the middle and southern portions of Australia for January of 2002 are significantly less than those for January of 2001. The decreases in water vapor amounts may be related to the eastward movement of the “warm pool” during the El Nino year. The waters north

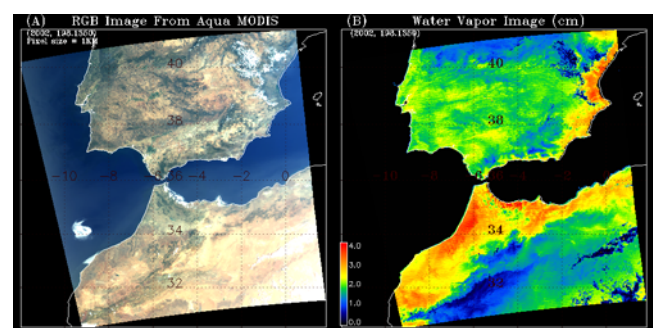


**Figure 8.** An example of water vapor retrievals from the Aqua MODIS near-IR channels. The left panel shows a false color image of a MODIS scene covering Spain, Morocco, and Algeria. The right panel shows the water vapor image derived from the Aqua MODIS near-IR channels. The MODIS data were acquired on 17 July 2002. The color scale maps water vapor from zero (blue) to 4.0 cm (red).

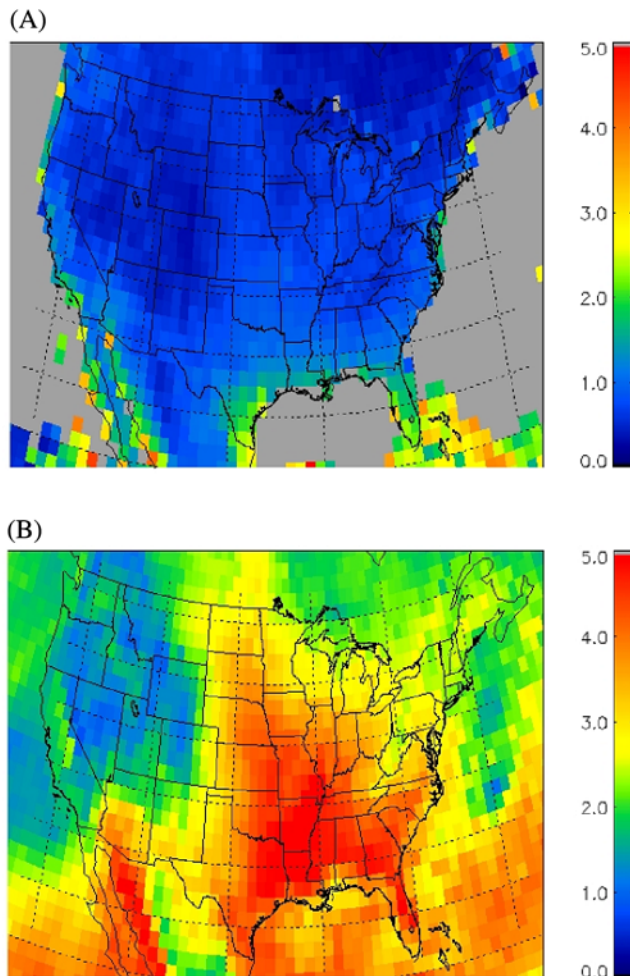


**Figure 9.** Monthly mean level 3 water vapor images over the continental United States, portions of Mexico and Canada for (a) January of 2001 and (b) July of 2001. The color scale on the right gives the total precipitable water vapor in centimeters.

of Australia in the Pacific Ocean are colder in the El Nino year. Less evaporation would occur and less amounts of water vapor would be available for transporting to the Australia continent.

#### 4.5. Sample Level 3 Global Water Vapor Images From Terra MODIS

[27] Figure 11a is a global water vapor image for January of 2001. During this Northern Hemisphere winter month, the water vapor amounts over most parts of North America, Europe, Asia, and northern part of the Africa Continent are small (<2 cm). Only the southern parts of Indian Continent and Indo-China have relatively higher moisture contents with column water vapor amounts in the range of 3–4.5 cm. Brazil, the southern part of African Continent, and Australia have high moisture contents. Figure 11b is a global water vapor image for July of 2001. The Northern Hemisphere becomes moister in comparison with the January image. The Indian Continent, Indo-China, and eastern part of China are now saturated with water vapor. The central United States is also quite

moist due to water vapor transported north from the Gulf of Mexico. The southern part of South America, southern part of the African Continent, and Australia are dry during their winter season. The high elevation areas, such as those of Rocky Mountains in North America, Andes Mountains in South America, Himalayas in Asia, and the Sahara desert areas in northern Africa have low moisture contents in both the July and January images. The water vapor images in Figures 11a and 11b show the utility of the level 3 monthly mean near-IR water vapor images for the studies of seasonal variations of water vapor on a global scale.

#### 5. Validation, Error Analysis, and Discussion

[28] We have made extensive analysis of the level 2 and level 3 near-IR water vapor images in order to make sure that no gross mistakes are present in our products. During the first year of Terra MODIS' operation in 2000, we made comparisons between our water vapor values and those obtained from ground-based upward looking Sun photometer measurements [Dubovik *et al.*, 2002]. The correlation

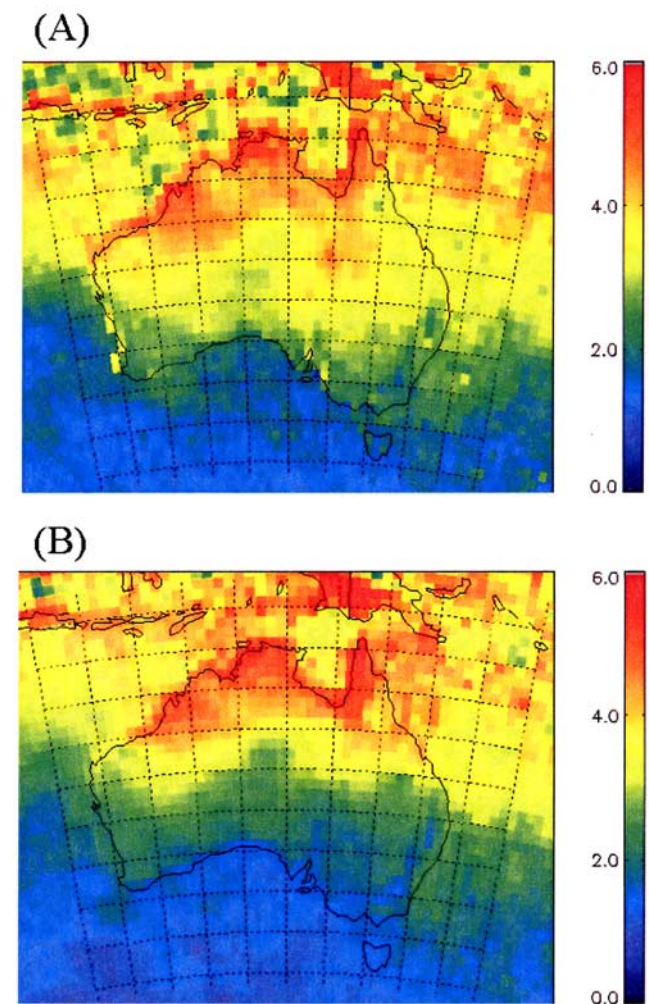


**Figure 10.** Monthly mean level 3 water vapor images over Australia for (a) January of 2001 and (b) January of 2002. The color scale on the right gives the total precipitable water vapor in centimeters.

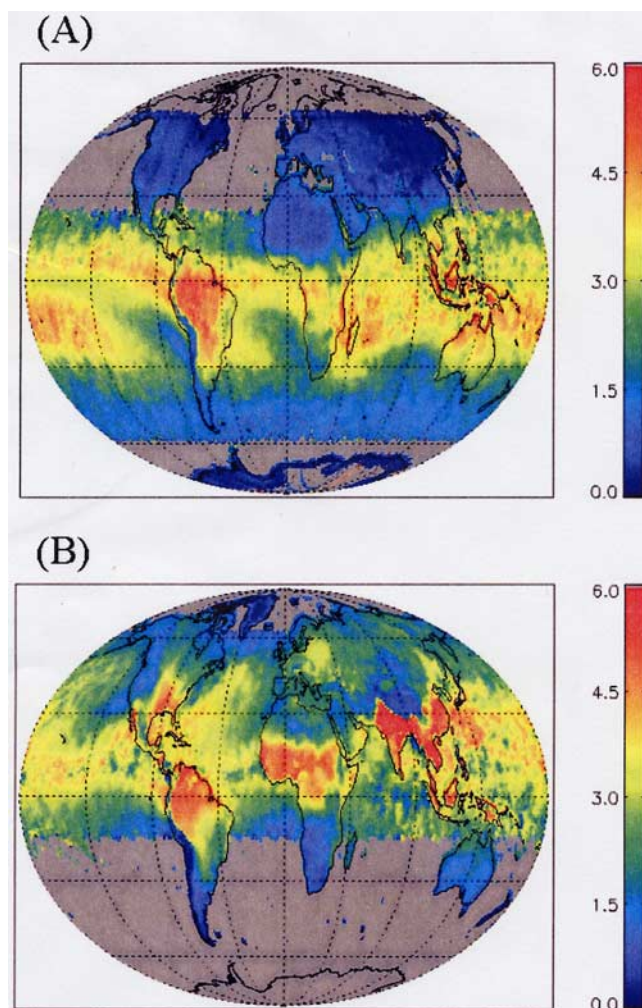


**Figure 11.** Monthly mean global level 3 water vapor images for (a) January of 2001 and (b) July of 2001. The color scale on the right gives the total precipitable water vapor in centimeters.

between the two sets of water vapor values is excellent. However, because systematic differences were present between the two water vapor retrieval algorithms, the water vapor values derived from the Sun photometer measurements were not used for the absolute validation of our MODIS near-IR water vapor products.

[29] In order to gain confidence in the accuracy of our near-IR water vapor products, we have compared the MODIS near-IR water vapor values with those measured with a ground-based upward looking microwave radiometer located at a site in the Southern Great Plains in Oklahoma for a time period between November 2000 and December 2001. The microwave radiometer measurements were sponsored by the Department of Energy's Atmospheric Radiation Measurement Program and the data were released for public use. Figure 12a shows a scatterplot between the water vapor values measured with the microwave radiometer and the MODIS near-IR water vapor values measured on clear days between November 2000 and December 2001. The data points for column water vapor amounts greater than 3.5 cm are not included in this plot. The regression

analysis of the two data sets gives a slope of 0.97 and a very small offset (0.06 cm), suggesting good agreement between the two sets of data. Figure 12b shows a similar plot but including the data points having column water vapor amounts greater than 3.5 cm for the same time period. The regression analysis of the two data sets gives a slope of 0.93. The decrease in the slope is largely due to the fact that for the few points with water vapor values greater than 3.5 cm, the MODIS water vapor values are somewhat systematically larger than the microwave radiometer water vapor values. Overall, the water vapor values from MODIS and from microwave radiometer measurements, as shown in Figures 12a and 12b, agree quite well, with differences typically in the range between 5 and 10%.

[30] Several sources of errors for water vapor retrievals from near-IR channels were previously studied [e.g., Gao et

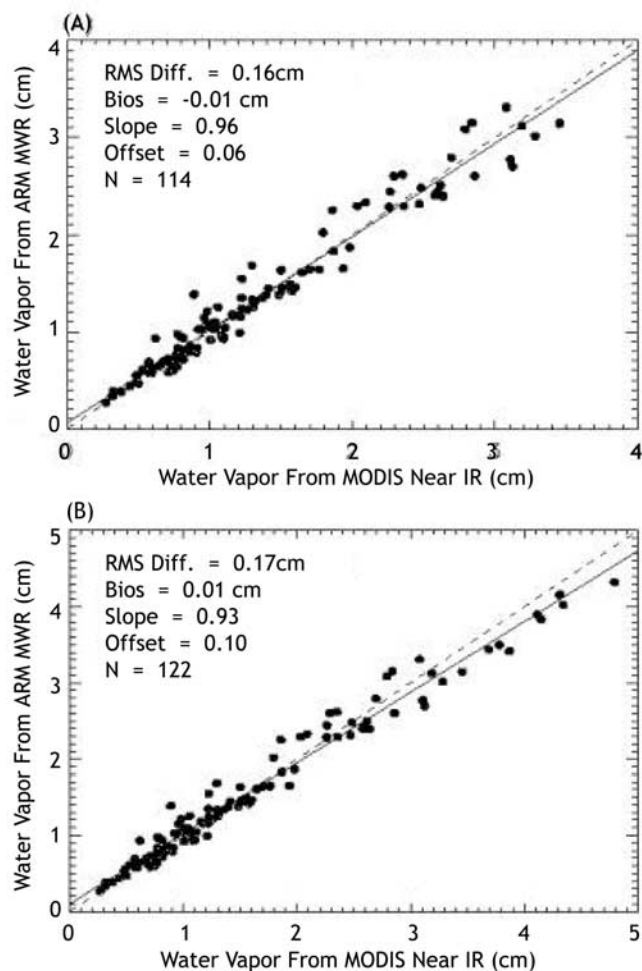


**Figure 12.** (a) Scatterplot between the water vapor values measured with a ground-based upward looking microwave radiometer at a site in the Southern Great Plains in Oklahoma and those retrieved from images of MODIS near-IR channels for a time period between November 2000 and December 2001 and for column water vapor amounts less than 3.5 cm; (b) similar to Figure 12a except that the data points for water vapor amounts greater than 3.5 cm are included in the analysis.

al., 1990; Kaufman and Gao, 1992; Gao et al., 1993; Bouffies et al., 1997]. They include uncertainties in the spectral reflectance of the surface, sensor radiometric and spectral calibrations, pixel registration between several channels, atmospheric temperature and moisture profiles, and the amount of haze. Through analysis of actual MODIS data, we have found that the largest sources of errors are the uncertainty in spectral reflectances of surface targets and the uncertainty in the amount of haze for dark surfaces. As described previously, we have assumed in our near-IR water vapor algorithm that the reflectance spectra of surface targets vary linearly with wavelength over the 0.8–1.3  $\mu\text{m}$  region (see Figures 2 and 3). The surface reflectances for the three water vapor absorption channels centered at 0.905, 0.936, and 0.94  $\mu\text{m}$  are obtained from the reflectances of the two atmospheric window channels at 0.865 and 1.24  $\mu\text{m}$  through linear interpolation. These predicted reflectances can deviate from the true reflectances of the surface targets. The amount of deviations depends on the surface targets. Under typical atmospheric conditions, the associated errors in column water retrievals for surfaces covered by green vegetation, dry vegetation, snow, mineral and soils (excluding iron-rich soils), and iron-rich soils are estimated [Gao et al., 1993] to be approximately 2.6%, 2.4%, 3.9%, 2.6%, and 8.4%, respectively.

[31] The effect of haze on remote sensing of water vapor depends on the amount of haze and the magnitude of the surface reflectances. Under typical atmospheric conditions with visibilities of 20 km or greater, the aerosol effects on water vapor retrievals are not significant for land surfaces with reflectance values of 0.2–0.4 in the 0.8–1.3  $\mu\text{m}$  spectral region. This is due to the self-compensation between the aerosol absorption and scattering effects [Fraser and Kaufman, 1985]. However, under hazy conditions (with visibilities less than 10 km) or when the surface reflectances near 1  $\mu\text{m}$  are small (less than about 0.1), errors can be 10% or slightly greater in our retrieved water vapor values using the atmospheric transmittance model if the aerosol effects are not corrected.

[32] Before the launch of Terra MODIS into space, we planned to correct for the aerosol effects in the level 2 near-IR water vapor product when the aerosol optical depths in the visible were 0.3 or greater. A module for aerosol corrections was developed and implemented in the near-IR water vapor algorithm. In this module, the level 2 aerosol optical depth image [Kaufman et al., 1997] and the water vapor image derived with the atmospheric transmittance model were read in. Scaling factors were derived using the aerosol optical depths and lookup table procedures. These scaling factors were then applied to the water vapor image to produce the final aerosol-effect-corrected water vapor image. Two precalculated lookup tables were used during the derivation of the scaling factors. The lookup tables were generated using DISORT, a radiative transfer code developed by Stamnes et al. [1988]. The k-distribution coefficients were used as inputs to DISORT in order to properly take care of water vapor absorption effects. Application of this aerosol correction module to real MODIS data did not yield improved estimates of water vapor values. As a result, we abandoned the efforts in correction of aerosol effects when retrieving water vapor values from the MODIS near-IR channels. Our level 2 near-

IR water vapor product is now derived simply using atmospheric transmittance models.

## 6. Summary

[33] We have developed an operational algorithm for retrieving column water vapor amounts from several MODIS near-IR channels. The algorithm relies on observations of water vapor attenuation of near-IR solar radiation reflected by surfaces or clouds. The algorithm uses the ratios of water vapor absorbing channels located within the 0.94- $\mu\text{m}$  water vapor band with the atmospheric window channels centered at 0.865  $\mu\text{m}$  and 1.24  $\mu\text{m}$ . The ratios largely remove the effects of the variation of surface reflectance with wavelength for most land surfaces and result in the atmospheric transmittances. The column water vapor amounts are derived from the transmittances using a table searching procedure. The lookup tables were generated with a line-by-line code and the HITRAN2000 line database. Typical errors in the derived water vapor values are estimated to be in the range between 5% and 10%. The daily level 2 “pixel-based” near-IR water vapor product, and the daily, 8-day, and monthly level 3 near-IR water vapor products at a 1° by 1° latitude-longitude grid globally are now routinely produced and archived at a NASA computing facility. These level 3 data products are useful for the study of seasonal and annual variations of water vapor on regional and global scales.

[34] **Acknowledgments.** The authors would like to thank many scientists and software engineers for their help and support during various stages of code development and integration. They include, but are not limited to, R. Hucek, V. Lin, R. R. Li, D. A. Chu, S. Mattoo, L. Remer, C. Ichoku, W. Han, P. Yang, S. H. Shen, M. A. Gray, E. G. Moody, P. A. Hubanks, Y. Han, P. Li, L. S. Rothman, A. Heidinger, and W. R. Ridgway at different organizations. This research is supported by the NASA Goddard Space Flight Center and by the Office of Naval Research.

## References

- Anderson, G. P., et al., MODTRAN4 radiative transfer modeling for remote sensing, *SPIE Proc.*, 4049, 176–183, 2000.
- Asrar, G., and R. Greenstone (Eds.), Mission to planet Earth/Earth Observing System reference handbook, NASA Goddard Space Flight Center, Greenbelt, Md., 1995.
- Berk, A., L. S. Bernstein, and D. C. Robertson, MODTRAN: A moderate resolution model for LOWTRAN7, *Rep. GL-TR-89-0122*, 42 pp., Air Force Geophys. Lab., Hanscom Air Force Base, Mass., 1989.
- Borel, C. C., W. B. Clodius, and J. Johnson, Water vapor retrieval over many surface types, *SPIE Proc.*, 2758, 218–228, 1996.
- Bouffies, S., F. M. Breon, D. Tanre, and P. Dubuisson, Atmospheric water vapor estimate by a differential absorption technique with the polarization and directionality of the Earth reflectances (POLDER) instrument, *J. Geophys. Res.*, 102, 3831–3841, 1997.
- Bowker, D. E., R. E. Davis, D. L. Myrick, K. Stacy, and W. T. Jones, Spectral reflectances of natural targets for use in remote sensing studies, *NASA Ref. Publ.*, 1139, 1985.
- Chesters, D. C., L. W. Uccellini, and W. D. Robinson, Low-level water vapor fields from the VISSR Atmospheric Sounder (VAS) “split-window” channels, *J. Clim. Appl. Meteorol.*, 22, 725–743, 1983.
- Condit, H. R., The spectral reflectance of American soils, *Photogramm. Eng.*, 36, 955–965, 1970.
- Conel, J. E., R. O. Green, C. Carrere, J. S. Margolis, R. E. Alley, G. Vane, C. J. Bruegge, and B. L. Gary, Atmospheric water vapor mapping with the airborne visible/infrared imaging spectrometer (AVIRIS) Mountain Pass, California, in *Proceedings of the Airborne Visible/Infrared Imaging Spectrometer (AVIRIS) Performance Evaluation Workshop*, edited by G. Vane, Publ. 88–38, pp. 21–29, Jet Propulsion Lab., Pasadena, Calif., 1988.
- Dubovik, O., B. Holben, T. F. Eck, A. Smirnov, Y. J. Kaufman, M. D. King, D. Tanre, and I. Slutsker, Variability of absorption and optical properties of key aerosol types observed in worldwide locations, *J. Atmos. Sci.*, 59, 590–608, 2002.

- Ferraro, R. R., F. Z. Weng, N. C. Grody, and A. Basist, An eight-year (1987–1994) time series of rainfall, clouds, water vapor, snow cover, and sea ice derived from SSM/I measurements, *Bull. Am. Meteorol. Soc.*, 77, 891–905, 1996.
- Fraser, R. S., and Y. J. Kaufman, The relative importance of aerosol scattering and absorption in remote sensing, *IEEE J. Geosci. Remotes. Sens.*, 23, 525–633, 1985.
- Frouin, R., P. Y. Deschamps, and P. Lecomte, Determination from space of atmospheric total water vapor amounts by differential absorption near 940 nm: Theory and airborne verification, *J. Appl. Meteorol.*, 29, 448–460, 1990.
- Gao, B.-C., and A. F. H. Goetz, Column atmospheric water vapor and vegetation liquid water retrievals from airborne imaging spectrometer data, *J. Geophys. Res.*, 95, 3549–3564, 1990.
- Gao, B.-C., E. R. Westwater, B. B. Stankov, D. Birkenheuer, and A. F. H. Goetz, Comparison of column water vapor measurements using downward looking near-infrared and infrared imaging spectrometer and upward looking microwave radiometers, *J. Appl. Meteorol.*, 31, 1193–1201, 1992.
- Gao, B.-C., A. F. H. Goetz, E. R. Westwater, J. E. Conel, and R. O. Green, Possible near-IR channels for remote sensing precipitable water vapor from geostationary satellite platforms, *J. Appl. Meteorol.*, 32, 1791–1801, 1993.
- Green, R. O., et al., Imaging spectrometry and the airborne visible infrared imaging spectrometer (AVIRIS), *Remote Sens. Environ.*, 65, 227–248, 1998.
- Hansen, J. E., and L. D. Travis, Light scattering in planetary atmospheres, *Space Sci. Rev.*, 16, 527–610, 1974.
- Kaufman, Y. J., and B.-C. Gao, Remote sensing of water vapor in the near IR from EOS/MODIS, *IEEE Trans. Geosci. Remote Sens.*, 30, 871–884, 1992.
- Kaufman, Y. J., D. Tanré, L. Remer, E. F. Vermote, D. A. Chu, and B. N. Holben, Operational remote sensing of tropospheric aerosol over the land from EOS-MODIS, *J. Geophys. Res.*, 102, 17,051–17,068, 1997.
- King, M. D., Y. J. Kaufman, W. P. Menzel, and D. Tanre, Remote sensing of cloud, aerosol, and water vapor properties from the Moderate Resolution Imaging Spectrometer (MODIS), *IEEE Trans. Geosci. Remote Sens.*, 30, 1–27, 1992.
- Kneizys, F. X., E. P. Shettle, L. W. Abreu, J. H. Chetwynd, G. P. Anderson, W. O. Gallery, J. E. A. Selby, and S. A. Clough, Users guide to LOW-TRAN 7, *AFGL-TR-8-0177*, Air Force Geophys. Lab., Bedford, Mass., 1988.
- Menzel, W. P., D. P. Wylie, and K. I. Strabala, Seasonal and diurnal changes in cirrus clouds as seen in four years of observations with the VAS, *J. Appl. Meteorol.*, 31, 370–385, 1992.
- Prabhakara, C., H. D. Chang, and A. T. C. Chang, Remote sensing of precipitable water over the oceans from Nimbus 7 microwave measurements, *J. Appl. Meteorol.*, 21, 59–68, 1982.
- Rothman, L. S., et al., The HITRAN molecular spectroscopic database and HAWKS (HITRAN Atmospheric Workstation): 1996 edition, *J. Quant. Spectrosc. Radiat. Transfer*, 60, 665–710, 1998.
- Salomonson, V. V., et al., MODIS: Advanced facility instrument for studies of the Earth as a system, *IEEE Trans. Geosci. Remote Sens.*, 27, 145, 1989.
- Stamnes, K., S.-C. Tsay, W. Wiscombe, and K. Jayaweera, Numerically stable algorithm for discrete-ordinate-method radiative transfer in multiple scattering and emitting layered media, *Appl. Opt.*, 27, 2502–2509, 1988.
- Stoner, E. R., and M. F. Baumgardner, Physiochemical, site and bidirectional reflectance factor characteristics of uniformly moist soils, 50 pp., *Rep. CR-160571*, NASA, Washington, D. C., 1980.
- Susskind, J., J. Rosenfield, and D. Reuter, Remote sensing of weather and climate parameters from HIRS2/MSU on TIROS-N, *J. Geophys. Res.*, 89, 4677–4697, 1984.
- Thai, S., and M. V. Schonermark, Determination of the column water vapor of the atmosphere using backscattered solar radiation measured by the Modular Optoelectronic Scanner (MOS), *Int. J. Remote Sens.*, 19, 3223–3236, 1998.
- Vane, G., R. O. Green, T. G. Chrien, H. T. Enmark, E. G. Hansen, and W. M. Porter, The Airborne Visible/Infrared Imaging Spectrometer, *Remote Sens. Environ.*, 44, 127–143, 1993.
- Vesperini, M., F.-M. Breon, and D. Tanre, Atmospheric water vapor content from spaceborne POLDER measurements, *IEEE Trans. Geosci. Remote Sens.*, 37, 1613–1619, 1999.
- Zhang, H., and W. P. Menzel, Improvement in thin cirrus retrievals using an emissivity-adjusted CO<sub>2</sub> slicing algorithm, *J. Geophys. Res.*, 107(D17), 4327, doi:10.1029/2001JD001037, 2002.

B.-C. Gao, Remote Sensing Division, Code 7212, Naval Research Laboratory, 4555 Overlook Avenue, SW, Washington, DC 20375, USA. (gao@nrl.navy.mil)

Y. J. Kaufman, Climate and Radiation Branch, NASA Goddard Space Flight Center, Greenbelt, MD 20771, USA.